Original

Shilyaeva, Y.I.; Bardushkin, V.V.; Gavrilov, S.A.; Silibin, M.V.;
Yakovlev, V.B.; Borgardt, N.I.; Volkov, R.L.; Smirnov, D.I.;
Zheludkevich, M.L.:

Melting temperature of metal polycrystalline nanowires electrochemically deposited into the pores of anodic aluminum oxide

PAPER

Melting temperature of metal polycrystalline nanowires electrochemically deposited into the pores of anodic aluminum oxide

Yu. I. Shilyaeva,[a] V. V. Bardushkin,[a] S. A. Gavrilov,[a] M. V. Silibin,*[a] V. B. Yakovlev,[a] N. I. Borgardt,[a] R. L. Volkov,[a] D. I. Smirnov[a] and M. L. Zheludkevich[bc]

The arrays of metallic nanowires are considered as promising precursors for 1D semiconductor nano-structures after appropriate treatment at temperatures close to the melting point. Therefore the melting behaviour of the metallic structures in oxide templates is a key parameter for the subsequent conversion process. The present paper focuses on understanding of the effect of mechanical stress generated during heating on the melting point of the metal nanowires deposited into the pores of anodic alumina. Extremely high local compressive stress appears due to the difference in the thermal coefficients of the oxide template and nanowires inside the pores. The effect of the composite structural parameter that may be related to the concentration of nanowires on the melting temperature has been investigated. A numerical model predicting the melting point has been developed for composites with indium, tin, and zinc nanowires. The simulation results obtained using the suggested model were compared with the experimental data.

1. Introduction

The arrays of metal nanowires represent an important class of one-dimensional nanostructures with properties very different from those of the corresponding bulk materials.[1] The investigation of properties of nanowires is of fundamental importance, and it is necessary from the point of view of their application. For example, the magnetic cobalt and nickel nanowires have great potential for high density data storage[2] and as materials for microwave applications.[3] The nanowires of noble metals are often considered for sensor applications[4] and as highly effective catalysts.[5] The arrays of nanowires of some fusible metals are relevant for thermoelectric systems[6] and have attracted considerable attention as precursors for one-dimensional semiconductor nanostructures[7–9] and core–shell structures.[10] Besides, fusible metal nanowires are often chosen as convenient objects for studying the thermodynamic properties. An appropriate thermochemical treatment of metal nanowires at temperatures close to their melting point is the way to get the desirable material. The resulting semiconductor nanostructures have a wide range of applications including nanoscale field-effect transistors,[11] nanolasers,[12] nanogenerators,[13] and many others.[14]

The ordered arrays of metal nanowires with a high aspect ratio, reproducible geometry, and a high degree of spatial order can be fabricated by electrochemical deposition into nanoporous templates of anodic aluminum oxide (AAO). This method is simple, cost-effective and can be performed at low temperature leading to wide usability.[15] However, the enclosure of particles inside the pores of an inert matrix is accompanied by additional phenomena associated with the presence of interfaces that affect the thermodynamic properties of nanostructures and require a detailed study.

Over the past two decades, a great number of nanowires of low melting point metals,[16,17] ferromagnetic metals,[16–18] and noble metals[5,17,19] were successfully fabricated using the AAO-templates. Characterization of formed structures typically includes X-ray diffraction (XRD) and scanning electron microscopy (SEM) analyses while studies of the thermal behavior are often only theoretical in nature. The experimental[20] and theoretical[21] aspects of thermal stability and temperature dependence of the mechanical properties[22] are addressed to a significantly lower extent. In the published papers related to the thermal characterization of metals inside the pores of the alumina matrix, the authors have presented the size dependence of the melting temperature.[20,23] At the same time, other geometric parameters such as the concentration of wires were not considered. Nevertheless, the actual structure of materials should be considered, since the

[a] *National Research University of Electronic Technology, Zelenograd, Moscow, Russia. E-mail: sil_m@mail.ru; Tel: +7-903-297-9141*

[b] *Institute of Materials Research, Helmholtz-Zentrum Geesthacht – Zentrum für Material-und Küstenforschung GmbH, Geesthacht, Germany*

[c] *Department of Materials and Ceramics Engineering, CICECO, University of Aveiro, Aveiro, Portugal*

placement of wire within an inert material is one of the ways to improve the stability of the nanoparticles.

In our previous papers we have shown that the actual structure of nanocomposites must be allowed for when conducting simulations.[24,25] In our previous studies the bulk density of the energy of deformation in composites with metallic nanowires in AAO was estimated and model calculations were performed.

The main aim of this work is to create a predictive model which can allow the numerical calculation of the melting temperature of the nanowire–AAO composites. In this study, we have synthesized highly ordered In, Sn, and Zn nanowire arrays within the pores of AAO membranes by electrochemical deposition. A series of samples with different diameters and concentrations of metallic wires have been investigated by differential scanning calorimetry (DSC) to assess the melting point.

The general assumption accepted in the model is that in a considered uniaxially reinforced nanocomposite the components are isotropic and the position of nanowires in the template is random. However, the material is assumed to be statistically homogeneous as a whole. This assumption results in the existence of an average distance between wires that may be related to the loading of the metal in the composite. Thus, the relation h/r is an important characteristic parameter of the nanocomposite structure (structural parameter). An averaged elementary volume can be considered as a regular hexagonal prism with one cylindrical nanowire oriented along the z axis in the centre. Some of these elementary volumes are schematically shown in Fig. 1a. Fig. 1b shows the cross-section of one elementary volume orthogonal to the z axis.

The concentration of the nanowires is considered by introducing appropriate structural parameters along with their diameter when modelling the melting processes. Thus, the model accounts for both the diameter of nanowires and the mechanical stress that originated from the difference in the thermal linear expansion coefficients (TLECs) of metals and the oxide matrix respectively. The observed melting behavior of embedded nanocrystals is then correlated with the suggested theoretical considerations. The presented model supported with experimental results will allow optimization of conditions for formation of semiconductor nanowires in the pores of the refractory matrix by additional post-treatment of metallic nanowires at temperatures close to their melting point.

2. Experimental

Anodic aluminum oxide was fabricated by using a two-step anodization process in a solution containing 40 g l^{-1} of oxalic acid as described elsewhere.[26] The obtained oxide samples were thoroughly washed and dried followed by treatment in a solution containing 3 wt% H_3PO_4 at 35–37 °C for 0, 15, 25, 35, and 45 min to form templates with different porosities.

Self-standing AAO membranes were obtained by dissolving the non-oxidized metallic Al in a mixture of 0.1 M $CuCl_2$ and 10 wt% HCl. The barrier layer was removed via immersion in 0.5 M NaOH solution for a short time. The conductive layer on the backside of alumina membranes was applied by deposition of a 100 nm thick Ti layer followed by a 200 nm thick Cu layer using PVD.

Metallic nanowire arrays have been prepared by electrochemical deposition inside the pores of the alumina matrix at ambient temperature in a galvanostatic mode, the current density was about 5 mA cm^{-2}. The composition of solutions[27] used for the electrodeposition process is given in Table 1.

Electrosynthesis was carried out using a two-electrode cell providing contact of the solution with the AAO matrix on one side only. The anode material was identical to the deposited metal. The process was continued until the moment when a metallic film appears on the surface, this film was then removed in the consequent step by gentle polishing. The samples were then rinsed with deionized water and dried in a nitrogen stream. Fig. 2 shows the flowchart of the AAO template-based fabrication of metallic nanowire arrays.

The structure of nanocrystal arrays in pores of the alumina matrix was characterized by X-ray diffraction analysis. Measurements were carried out using the multifunction X-ray unit «X-Ray MiniLab» operating in a diffraction mode. Samples were studied in the $\Theta - 2\Theta$ scan mode with a wavelength λ (CuKα) = 1.54 Å using Bragg–Brentano focusing.

Morphology of formed structures was investigated by scanning electron microscopy. Measurements were carried out using the Helios NanoLab 650.

Thermal properties of the obtained composites were characterized using a differential scanning calorimeter DSC 204 F1 Phoenix (Netzsch). Heating of samples (3–5 mg) was carried out in aluminum crucibles at a rate of 10 K min^{-1} under an argon atmosphere. Empty Al crucibles were used as references.
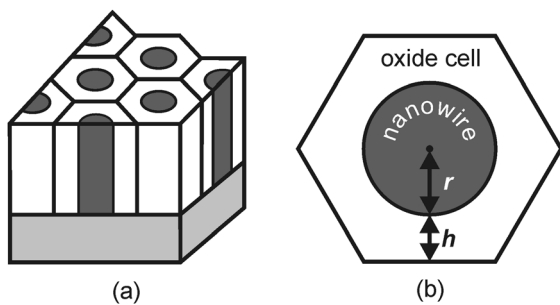

Fig. 1 Schematic representation of the composite structure: (a) several elementary volumes and (b) an elementary volume in the cross-sectional plane.

Table 1 Solutions used for electrodeposition of different metals

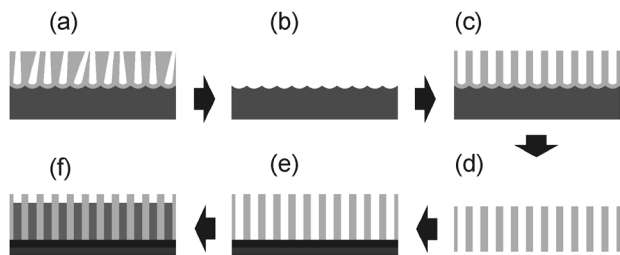| Metal	Components	Concentration (g l^{-1})
Indium	$In_2(SO_4)_3$	150
	$Na_2SO_4 \cdot 10H_2O$	10
Tin	$SnSO_4$	40
	H_2SO_4	100
Zinc	$ZnSO_4$	300
	H_2SO_4	10

Fig. 2 Schema of the nanowire array fabrication process by electrode-position: (a) first step anodizing of aluminum, (b) removal of the low ordered oxide layer, (c) second step anodizing of aluminum, (d) removal of unreacted aluminum and the barrier oxide layer, (e) deposition of the conductive layer, and (f) electrochemical growth of metal nanowires.

3. Results

Fig. 3 shows the top view and the cross-sectional view of AAO membranes filled with tin nanowires.

One can see that the deposited metal completely fills the pores. In this case the diameter of the nanowire is assumed to be equal to the inner pore diameter. Values of the pore radius and the structural parameter of the alumina matrix were determined from the microscope data using statistical analysis of micrographs taken on the sample surfaces. Fig. 4 illustrates

Fig. 5 X-ray diffractograms of In (a), Sn (b), and Zn (c) nanowire arrays in the AAO membranes.

the change in the character of the structural parameter and the pore radius depending on the time of treatment with a 3 wt% H_3PO_4 solution.

The structure of obtained In, Sn, and Zn nanowire arrays embedded in the AAO membranes was studied using XRD. Fig. 5 shows X-ray diffractograms of the respective samples. The obtained diffractograms clearly demonstrate the presence of electrodeposited metals (In, Sn, Zn) as well as peaks which correspond to unetched aluminum remnants.

The analysis of XRD results do not show any signs of strong texturing of polycrystallites in the pores. The wide signal in the range of 2Θ angles up to $30°$ is associated with the scattering of X-rays on the amorphous porous alumina matrix.

Fig. 6 shows DSC heating curves of composites with different values of the structural parameter h/r. DSC analysis was also performed on an empty AAO membrane and electrochemically deposited bulk films of indium, tin, and zinc for the correct comparison of the temperature effects observed for the metal filled AAO membranes.

No thermal effects were detected on the DSC curve of the empty AAO membrane. Heating curves of bulk metal probes are also shown in Fig. 6.

The melting point was determined from the onset temperature of the endothermic peak. Melting temperature of indium, tin, and zinc nanowires was analyzed for composites having different loadings of metals determined by controlling the geometrical parameters.

It can be clearly seen that the melting temperature of nanowires embedded in the oxide matrix is remarkably lower than that of the bulk metal. There is also a well-defined trend
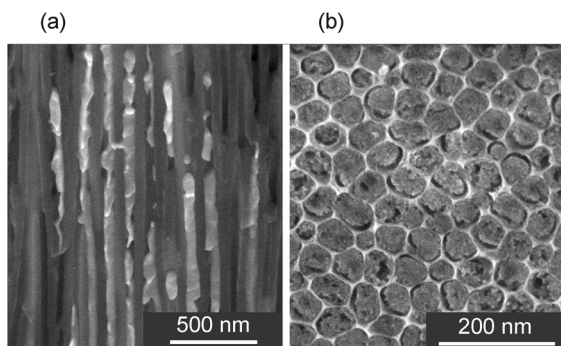

Fig. 3 SEM cross-sectional view (a) and top view (b) of the AAO–Sn composite.
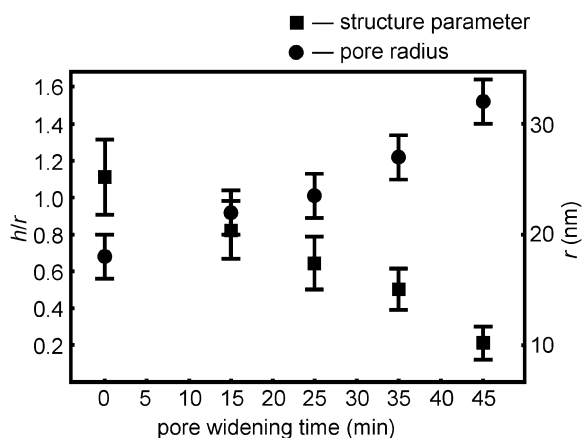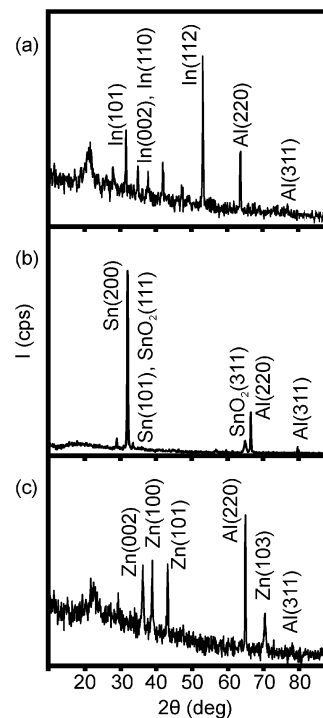

Fig. 4 Dependence of the structural parameter and the pore radius of the alumina template on etching time in H_3PO_4 solution.

19396 | Phys. Chem. Chem. Phys., 2014, 16, 19394–19401

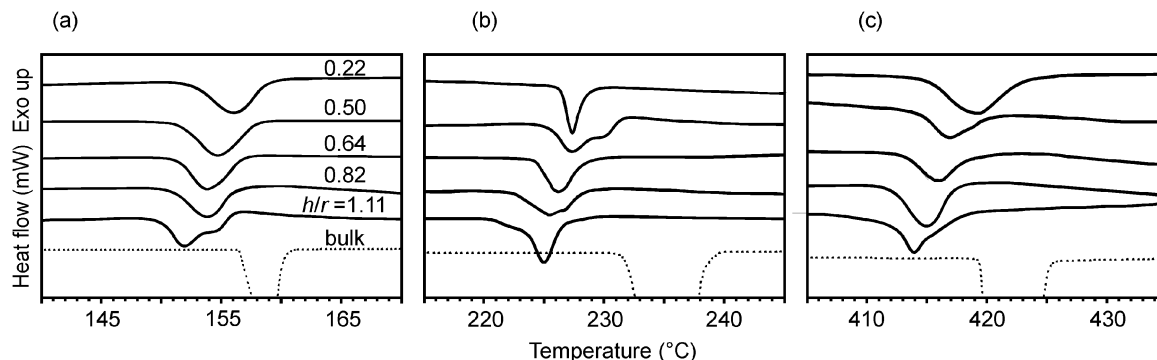This journal is © the Owner Societies 2014

Fig. 6 DSC curves of composites with (a) indium, (b) tin, and (c) zinc nanowires with various values of the structural parameter h/r. Curves marked "bulk" correspond to bulk metal film electrodeposited under similar conditions.

showing a decrease of the melting point with an increase of the structural parameter h/r for all the metals under study.

4. Model

The following tasks should be resolved first when creating a model predicting the melting point of metallic nanowires electrochemically deposited into AAO pores:

(a) to correlate the distance between the wires with structural parameters that can be measured directly,

(b) to derive mathematical formulas convenient for numerical analysis without losing information about the structure of the composite.[28,29]

One can assume that each nanowire has an average radius r and the distance from the center of a regular hexagon to its side is $r + h$ (see Fig. 1b). The base area of the elementary cell is then $S = 2\sqrt{3}(r + h)^2$, and the cross sectional area of the wire is $S_{\mathrm{w}} = \pi r^2$. Defining the concentration of wires as $\nu_{\mathrm{w}} = S_{\mathrm{w}}/S$, we have

$$\nu_{\mathrm{w}} = \frac{\pi}{2\sqrt{3}(1 + h/r)^2}, \quad \nu_{\mathrm{m}} = 1 - \nu_{\mathrm{w}}.$$

The index "w" here and below denotes the values related to the metallic wires, while "m" indicates those related to the matrix.

The characteristic parameter defining the structure of the composite can thus be represented by the concentration of nanowires as

$$\frac{h}{r} = \sqrt{\frac{\pi}{2\sqrt{3} \cdot \nu_{\mathrm{w}}}} - 1. \tag{1}$$

It is evident that the maximum theoretical value of the concentration of nanowires is observed when $h/r \to 0$, which corresponds to $\nu_{\mathrm{w}} \to \dfrac{\pi}{2\sqrt{3}} \approx 0.9$.

The minimum value of the concentration of wires is observed when $h/r \to \infty$; hence, $\nu_{\mathrm{w}} \to 0$. This range of concentrations for nanowires corresponds to the boundaries of the applicability of the suggested approach for simulation of such materials.

Derivation of model

The melting point T_{m} of the cluster enclosed in a refractory matrix can be described by the following equation:[30,31]

$$\frac{T_{\mathrm{m}} - T_{\mathrm{m},\infty}}{T_{\mathrm{m},\infty}} = \frac{1}{\Delta H_{\mathrm{m},\infty}}\left(\Delta E + (\sigma_{\mathrm{lm}} - \sigma_{\mathrm{sm}})\frac{A}{V}\right), \tag{2}$$

where $T_{\mathrm{m},\infty}$ (K) is the melting point of the corresponding bulk material; $\Delta H_{\mathrm{m},\infty}$ (J m^{-3}) is fusion enthalpy; ΔE (J m^{-3}) is strain energy density resulting from the volume change upon melting; σ_{lm} and σ_{sm} (J m^{-2}) are liquid/matrix and solid/matrix interface energies, respectively; and A/V (m^{-1}) is the parameter accounting for the form of the nanowire and is equal to the ratio of surface area to volume.[31] Formula (2) will be further used to calculate the melting temperature of metallic nanowires enclosed in the pores of the alumina matrix. The A/V ratio for the cylindrical shape wire is:

$$\frac{A}{V} = \frac{2}{r} + \frac{2}{L},$$

where r is the radius of the nanowire in the cross-sectional plane and L is the length of the nanowire.

The term $2/L$ can be neglected since the length of the nanowires in the experiment is about 30 microns. Then eqn (2) can be transformed into the following form:

$$\frac{T_{\mathrm{m}} - T_{\mathrm{m},\infty}}{T_{\mathrm{m},\infty}} = \frac{1}{\Delta H_{\mathrm{m},\infty}}\left(\Delta E + \frac{2(\sigma_{\mathrm{lm}} - \sigma_{\mathrm{sm}})}{r}\right). \tag{3}$$

The next step is to perform a more detailed description of the calculation of each parameter included in eqn (3). The average values of the surface energies can be used as the interphase energies of melt/matrix σ_{lm} and nanocrystal/matrix σ_{sm}:

$$\sigma_{\mathrm{lm}} = \frac{\sigma_{\mathrm{Al_2O_3}} + \sigma_{\mathrm{l}}}{2}, \quad \sigma_{\mathrm{sm}} = \frac{\sigma_{\mathrm{Al_2O_3}} + \sigma_{\mathrm{s}}}{2}, \tag{4}$$

where $\sigma_{\mathrm{Al_2O_3}} = 169$ mN m^{-1} is specific surface energy of anodic alumina;[32] σ_{l} and σ_{s} are specific surface energies of liquid and solid metals near the melting point, respectively[31,32] (Table 2). The heats of fusion[31,32] for considered metals are also given in Table 2.

This journal is © the Owner Societies 2014

Phys. Chem. Chem. Phys., 2014, **16**, 19394–19401 | **19397**

Table 2 Specific surface energies σ_l, σ_s and fusion enthalpy $\Delta H_{m,\infty}$ of metals

Metal	σ_l (mN m^{-1})	σs (mN m^{-1})	$\Delta H_{m,\infty}$ (MJ m^{-3})
Indium	566	633	210
Tin	515	680	430
Zinc	650	830	790

Table 3 Thermoelastic characteristics of composite components

Material	Young's modulus E (GPa)	Poisson's ratio μ	$T_{m,\infty}$ (K)	$\alpha_{\parallel} \times 10^6$ (K^{-1})	$\alpha_{\perp} \times 10^6$ (K^{-1})
Indium	10.5	0.46	429.6	−42.0 (400 K)	79.5 (400 K)
Tin	48	0.33	504.9	41.4 (500 K)	20.3 (500 K)
Zinc	115	0.325	692.6	50.3 (650 K)	27.9 (650 K)
Alumina	140	0.32	1273^a	6.46 (400 K)	5.82 (400 K)
				7.38 (600 K)	6.68 (600 K)
				7.99 (800 K)	7.23 (800 K)

Note: $\alpha_{\parallel}$ and $\alpha_{\perp}$ are the values of TLECs parallel and perpendicular to the z axis (wire), respectively. ^{a} Temperature corresponding to the beginning of geometric parameter changes in alumina.

The strain energy density, ΔE, is determined by the mechanical stress caused by the difference between the TLECs of nanowires and the matrix.[30] The correct definition of ΔE is one of the main problems that arise when building up a prediction model. Below, the solution of the model equation is described in a step by step way.

First of all, the data on the thermoelastic properties of composite components are required. Detailed information about these characteristics is known from the literature[33–37] as given in Table 3.

The derivation of equation for ΔE is based on the generalized singular approximation of random field theory.[38] From the physical point of view, using this approximation is equivalent to the assumption about homogeneity of physicomechanical fields within the individual element in a composite medium. The strain energy density ΔE is defined as the value resulting from the averaging procedure:

$$\Delta E = \nu_w E_w + \nu_m E_m, \tag{5}$$

where E_w and E_m are appropriate energies in the wire and matrix respectively.

The bulk strain energy density $E(\mathbf{r})$ is one of the most important local physicomechanical characteristics of heterogeneous media. Here, $\mathbf{r}$ is the radius vector of a random point in the medium; $E(\mathbf{r}) = E_w$, in the wire and $E(\mathbf{r}) = E_m$, in the matrix. $E(\mathbf{r})$ is defined as:[28,29]

$$E(\mathbf{r}) = \tfrac{1}{2}\varepsilon_{ij}(\mathbf{r})\sigma_{ij}(\mathbf{r}), \quad i,j = 1, 2, 3. \tag{6}$$

The composition of tensors of deformation $\varepsilon_{ij}(\mathbf{r})$ and strain $\sigma_{ij}(\mathbf{r})$ considers the contraction on the corresponding indices. Adequate simulation of the laws of change in $E(\mathbf{r})$ enables the correct prediction of their behavior under loading conditions (critical in particular) in designing materials. It can give

recommendations for the choice of component compositions and their concentrations.

Using the generalized Hook's law

$$\varepsilon_{ij}(\mathbf{r}) = s_{ijkl}(\mathbf{r})\sigma_{kl}(\mathbf{r}), \quad i, j, k, l = 1, 2, 3,$$

where $s_{ijkl}(\mathbf{r})$ are components of compliance tensor s; eqn (6) for $E(\mathbf{r})$ can be written as

$$E(\mathbf{r}) = \tfrac{1}{2}s_{ijkl}(\mathbf{r})\sigma_{kl}(\mathbf{r})\sigma_{ij}(\mathbf{r}). \tag{7}$$

The basis for analysis of the distribution of the local values of elastic energy is determining the relationship between strain $\sigma_{ij}(\mathbf{r})$ in one element and the average (external) strain $\langle\sigma_{kl}(\mathbf{r})\rangle$ applied to the entire composite. The most convenient characteristic which enables performing this analysis is the operator of strain concentration $K^\sigma(\mathbf{r})$ (a fourth-order tensor) with components $K^\sigma_{ijkl}(\mathbf{r})$:[28,29,39–41]

$$\sigma_{ij}(\mathbf{r}) = K^\sigma_{ijkl}(\mathbf{r})\langle\sigma_{kl}(\mathbf{r})\rangle. \tag{8}$$

Eqn (7) can then be rewritten as

$$E(\mathbf{r}) = \tfrac{1}{2}s_{ijkl}(\mathbf{r})K^\sigma_{klmn}(\mathbf{r})\langle\sigma_{mn}(\mathbf{r})\rangle K^\sigma_{ijpq}(\mathbf{r})\langle\sigma_{pq}(\mathbf{r})\rangle. \tag{9}$$

The suggested approach which related the assessment of the local stress–strain state of an inhomogeneous medium using the operator $K^\sigma(\mathbf{r})$ is convenient because it allows us to exclude information about external mechanical action due to the fact that $K^\sigma(\mathbf{r})$ is only dependent on the parameters of the medium and the material structure.[28,29,39–41]

The equations for the equilibrium of an elastic heterogeneous medium must be solved for the correct analysis of the local stress concentration in the composite enabling us to take into account the interaction of elements of heterogeneity, composition and structure of the material, shape and concentration of inclusions. However, in general, it is impossible to derive the relation for numerical calculations $K^\sigma(\mathbf{r})$. Therefore, various approximations are used for its calculation. Within the framework of generalized singular approximation only the singular component of Green's tensor of equations for the equilibrium is used. It depends only on the Dirac delta function. A homogeneous reference body whose material constants are included in the final expression for calculating $K^\sigma(\mathbf{r})$ is also introduced. In this case, the equation for $K^\sigma(\mathbf{r})$ has the following form (indices here and below are omitted for convenience whenever possible):[28,29]

$$K^\sigma(\mathbf{r}) = c(\mathbf{r})(I - gc''(\mathbf{r}))^{-1}\langle c(\mathbf{r})(I - gc''(\mathbf{r}))^{-1}\rangle^{-1}, \tag{10}$$

where I is a unit tensor of the fourth order; c is the elasticity modulus tensor; fourth-order tensor g is an integral from a singular component of the second derivative of Green's tensor for equations of equilibrium. The double primes indicate the difference between the corresponding parameters of a heterogeneous medium and a homogeneous reference body, characteristics of which are denoted by the superscript "ref": $c''(\mathbf{r}) = c(\mathbf{r}) - c^{\text{ref}}$. The angular parentheses here and below determine the procedure for averaging which for some random variable

19398 | *Phys. Chem. Chem. Phys.*, 2014, **16**, 19394–19401

This journal is © the Owner Societies 2014

$a(\mathbf{r})$ in the case of the composite containing matrix and isotropic inclusions is reduced to summing

$$\langle a(\mathbf{r}) \rangle = \nu_w a_w + \nu_m a_m, \qquad (11)$$

where $\nu_w + \nu_m = 1$.[28,29,42]

Components g_{ijkl} of g tensor can be calculated upon knowing components a_{ijkl} of the fourth-rank tensor A as the following:

$$a_{iklj} = -\frac{1}{4\pi}\int n_k n_j t_{il}{}^{-1} \mathrm{d}\Omega, \qquad (12)$$

and then symmetrization is performed using pairs of i and j and k and l indices.[38]

In eqn (12), $\mathrm{d}\Omega = \sin\theta\,\mathrm{d}\theta\,\mathrm{d}\varphi$ is an element of the solid angle in a spherical system of coordinates; $t_{il}{}^{-1}$ are the elements of the reverse matrix T with elements $t_{il} = c_{iklj}^{\mathrm{ref}} n_k n_j$; n_k and n_j $(k, j = 1, 2, 3)$ are components of a vector of an external normal to the inclusion's surface. For ellipsoidal inclusions with principal semiaxes l_1, l_2, and l_3 the components of the normal vector are determined by the relationship:

$$n_1 = \frac{1}{l_1}\sin\theta\cos\varphi,\ n_2 = \frac{1}{l_2}\sin\theta\sin\varphi,\ n_3 = \frac{1}{l_3}\cos\theta.$$

For the matrix structure, the parameters of the reference body can be considered to correspond to the respective characteristics of the matrix.[42]

When considering inclusions in the form of nanowires with principal semiaxes $l_1 = l_2 = r$, $l_3 \to \infty$, the following relation will be satisfied for the components of the normal vector:

$$n_1 = \frac{1}{r}\sin\theta\cos\varphi,\ n_2 = \frac{1}{r}\sin\theta\sin\varphi,\ n_3 \to 0.$$

The elastic characteristics of the matrix can be taken as the parameters of the reference body. Then in eqn (10), $c''(\mathbf{r}) = c(\mathbf{r}) - c_m$, and $c''(\mathbf{r}) = c_w - c_m$ in calculations for the nanowires and $c''(\mathbf{r}) = 0$ for the matrix. Considering eqn (5), the equation for a strain concentration operator in the nanowire would take the form:[28,29]

$$K_w^\sigma = c_w(I - g(c_w - c_m))^{-1} \times (\nu_w c_w(I - g(c_w - c_m))^{-1} + \nu_m c_m)^{-1}. \qquad (13)$$

The equivalent equation for a strain concentration operator in the matrix has the following form:

$$K_m^\sigma = c_m(\nu_w c_w(I - g(c_w - c_m))^{-1} + \nu_m c_m)^{-1}. \qquad (14)$$

Eqn (13) and (14) are used for further model calculations of the bulk strain energy density $E(\mathbf{r})$ (in the wires and the matrix) using formula (9). Furthermore, the operator of strain concentration $K^\sigma(\mathbf{r})$ will be used for deriving the formula for predicting the value of the average stress $\langle\sigma_{kl}(\mathbf{r})\rangle$ that originated from the difference between the TLECs of isotropic components of the uniaxially reinforced composite.

The next step is to derive the relation for calculating $\langle\sigma_{kl}(\mathbf{r})\rangle$ which in turn can be used for calculation of $E(\mathbf{r})$ using formula (9).

It should be noted that for real inhomogeneous media, operator $K^\sigma(\mathbf{r})$ is nondegenerate.[28,29] Therefore, using the inverse of the $K^\sigma(\mathbf{r})$ tensor, one can calculate the average stress $\langle\sigma_{kl}(\mathbf{r})\rangle$. The local stress then has the following form:

$$\sigma_{ij}(\mathbf{r}) = c_{ijkl}(\mathbf{r})\alpha_{kl}(\mathbf{r})\Delta T.$$

Here, $\alpha_{kl}(\mathbf{r})$ are the thermal expansion tensor components and ΔT is the temperature change. The following expression can be written for a composite with isotropic components:

$$\alpha_{kl}(\mathbf{r}) = \alpha(\mathbf{r})\delta_{kl},$$

where $\alpha(\mathbf{r})$ is the thermal expansion coefficient, with $\alpha(\mathbf{r}) = \alpha_m$ for the matrix and $\alpha(\mathbf{r}) = \alpha_w$ for the inclusions, and δ_{kl} is the Kronecker symbol. The contribution of the local stress state of an individual inclusion to the average stress state of the composite is then

$$\langle\sigma_w\rangle = (K_w^\sigma)^{-1}\sigma_w = (K_w^\sigma)^{-1} c_w \alpha_w \Delta T\delta_{kl}.$$

For an individual infinitesimal volume of matrix, the contribution of the local stress state to the average stress state of the composite is

$$\langle\sigma_m\rangle = (K_m^\sigma)^{-1}\sigma_m = (K_m^\sigma)^{-1} c_m \alpha_m \Delta T\delta_{kl}.$$

Taking into account eqn (11), the average stress induced by the thermal expansion of the uniaxially reinforced composite with isotropic components can be defined as:

$$\langle\sigma_{ij}(\mathbf{r})\rangle = \nu_w\langle\sigma_w\rangle + \nu_m\langle\sigma_m\rangle, \text{ or}$$
$$\langle\sigma_{ij}(\mathbf{r})\rangle = (\nu_w(K_w^\sigma)^{-1} c_w \alpha_w + \nu_m(K_m^\sigma)^{-1} c_m \alpha_m)\Delta T\delta_{kl}. \quad (15)$$

ΔE can be calculated using relation (5) when the volume concentration of wires in the composite and relations (13)–(15) for calculations $E(\mathbf{r}) = E_w$ and $E(\mathbf{r}) = E_m$ (according to formula (9)) are known.

Thus, the model built for metal nanowires–AAO composites allows us to take into account the radius of wires and their concentration and can be used for modeling thermoelastic characteristics[24,25,43,44] as well as melting processes of nanowires embedded in a refractory matrix (see (3)).

Numerical calculations

The tensors written in the matrix form were employed in the numerical calculations. The nonzero elements c_{ij} $(i, j = 1,\ldots,6)$ of the elastic modulus tensor c for an isotropic material can be expressed through its Young's modulus E and Poisson's ratio μ:[38]

$$c_{11} = c_{22} = c_{33} = \frac{E(1 - \mu)}{(1 + \mu)(1 - 2\mu)};$$

$$c_{44} = c_{55} = c_{66} = \frac{E}{2(1 + \mu)};$$

$$c_{12} = c_{13} = c_{23} = \frac{E\mu}{(1 + \mu)(1 - 2\mu)}.$$

At first, model calculations of the strain concentration operator for matrix and wires depending on the structural

This journal is © the Owner Societies 2014

Phys. Chem. Chem. Phys., 2014, **16**, 19394–19401 | **19399**
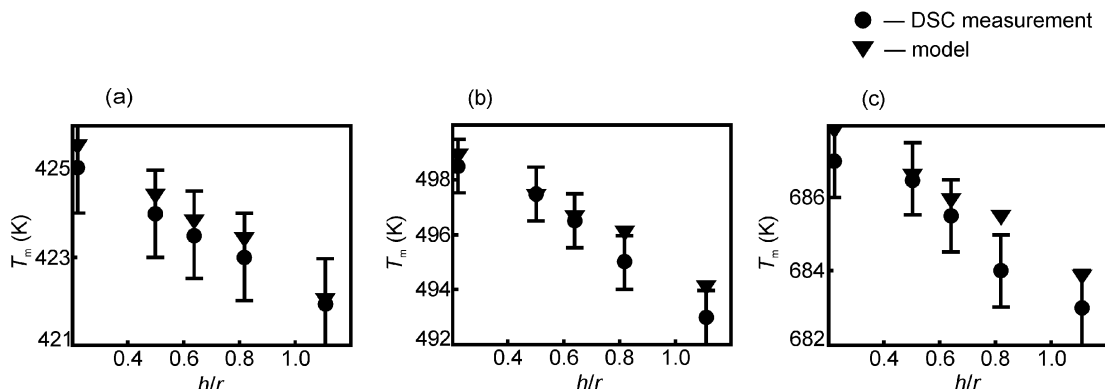
● — DSC measurement
▼ — model

Fig. 7 Results of numerical modeling of T_m in comparison with experimental values for (a) indium, (b) tin, and (c) zinc nanowire arrays in the AAO matrix.

parameter h/r were carried out using formulas (13) and (14). The results of numerical modeling of stress and strain concentration operators for these materials are published elsewhere.[44] Furthermore, for the same composites the model calculations of the average stress $\langle \sigma_{kl}(\mathbf{r}) \rangle$ were performed using relation (15) on the basis of calculated dependence of stress concentration operator components on h/r. Calculations of $\langle \sigma_{kl}(\mathbf{r}) \rangle$ were performed at $T \approx T_{m,\infty}$ K, $\Delta T = 20$ K in perpendicular and parallel directions to the wires. Here, the values $\alpha_{\parallel}$ and $\alpha_{\perp}$ were firstly subjected to the procedure of linearization of available data given in Table 3. For example, the calculated value $\alpha_{\parallel}$ for Al_2O_3 at 500 K (a temperature close to $T_{m,\infty}$ of tin) is the arithmetical mean of its values at 400 K and 600 K given in Table 3, *i.e.* $\alpha_{\parallel} = 6.92 \times 10^{-6}$ K^{-1}. Then, calculated in this way values $\alpha_{\parallel}$ and $\alpha_{\perp}$ for each material were averaged using the following formula:

$$\alpha = \frac{2\alpha_{\perp} + \alpha_{\parallel}}{3}.$$

Exactly these averaged values α_w and α_m were used in model calculations carried out using relation (15). The results of numerical modeling of $\langle \sigma_{kl}(\mathbf{r}) \rangle$ for these materials have been presented earlier.[24] Note that it is necessary to know for the calculation of $E(\mathbf{r})$ according to formula (9) the values of the elements $s_{ij}(i, j = 1, \ldots, 6)$ of s matrix of compliance tensor. To get s_{ij} one should use the fact that $s = c^{-1}$.[42] The results of numerical modeling of $E(\mathbf{r})$ for these materials have been also reported previously.[25]

Data presented in Tables 2 and 3 combined with σ_{lm}, σ_{sm}, and ΔE values calculated using eqn (4) and (5) were used to calculate melting temperature T_m using formula (3) for indium, tin, and zinc nanowires electrochemically deposited into the AAO pores. The results of numerical modeling of T_m depending on the structural parameter h/r are given in Fig. 7. The h/r values used for the calculations correspond to the real structures measured experimentally by DSC. A good agreement can be observed between the measured melting temperatures and ones calculated using the suggested model.

5. Conclusions

The theoretical model for melting temperature dependence on the structural parameters of metal nanowires embedded in anodic oxide pores is developed. The model takes into account

the concentration of metallic wires and strain energy caused by mechanical stress that resulted from the difference between the TLECs of nanocrystals and the matrix. Model numerical calculations for embedded indium, tin, and zinc nanowire arrays in the pores of anodic aluminum oxide have been performed on the basis of the proposed model.

The ordered arrays of indium, tin, and zinc nanowires with different geometrical parameters have been synthesized by electrochemical deposition. Melting of nanocrystals enclosed in the AAO matrix was investigated by differential scanning calorimetry. The effect of the structural parameter on the melting point of embedded indium, tin, and zinc nanowires has been experimentally determined showing a decrease of the melting temperature for nanowires with lower diameter.

The appropriateness of the suggested model is confirmed by results of comparative analysis of experimental and calculated data, which showed satisfactory agreement of model calculations and measured values of the melting point.

The proposed model of physical and mechanical properties and thermal stability ranges of nanowires in oxide templates will allow us to optimize the processes of production and exploitation of nanocomposites based on AAO.

Acknowledgements

References

1 J. T. Hu, T. W. Odom and C. M. Lieber, *Acc. Chem. Res.*, 1999, **32**, 435–445.

2 J. Sarkar, C. G. Khan and A. Basumallick, *Bull. Mater. Sci.*, 2007, **30**, 271–290.

3 D. J. Sellmyer, M. Zheng and R. Shomski, *J. Phys.: Condens. Matter*, 2001, **13**, R433–R460.

4 G. Kartopu, S. Habouti and M. Es-Souni, *Mater. Chem. Phys.*, 2008, **107**, 226–230.

19400 | *Phys. Chem. Chem. Phys.*, 2014, **16**, 19394–19401

This journal is © the Owner Societies 2014

5 H. Wang, C. Xu, F. Cheng and S. Jiang, *Electrochem. Commun.*, 2007, **9**, 1212–1216.

6 Y. M. Lin, X. Sun and M. S. Dresselhaus, *Phys. Rev. B: Condens. Matter Mater. Phys.*, 2000, **62**, 4610–4623.

7 J. Fan, T. Gao, G. Meng, Y. Wang, X. Liu and L. Zhang, *Mater. Lett.*, 2002, **57**, 656–659.

8 S. Gavrilov, L. Nosova, I. Sieber, A. Belaidi, L. Dloczik and Th. Dittrich, *Phys. Status Solidi A*, 2005, **202**(8), 1497–1501.

9 Y. T. Lin, J. B. Shi, Y. C. Chen, C. J. Chen and P. F. Wu, *Nanoscale Res. Lett.*, 2009, **4**, 694–698.

10 L. Li, Y. W. Yang, G. H. Li and L. D. Zhang, *Small*, 2006, **2**(4), 548–553.

11 X. Duan, Y. Huang, Y. Cui, J. Wang and C. M. Lieber, *Nature*, 2001, **409**, 66–69.

12 M. H. Huang, S. Mao, H. Feick, H. Q. Yan, Y. Y. Wu, H. Kind, E. Weber, R. Russo and P. D. Yang, *Science*, 2001, **292**, 1897–1899.

13 Z. L. Wang and J. H. Song, *Science*, 2006, **312**, 242–246.

14 C. M. Lieber and Z. L. Wang, *MRS Bull.*, 2007, **32**, 99–108.

15 O. Jessensky, F. Müller and U. Gösele, *Appl. Phys. Lett.*, 1998, **72**, 1173–1175.

16 A. J. Yin, J. Li, W. Jian and A. J. Bennett, *Appl. Phys. Lett.*, 2001, **79**, 1039–1041.

17 A. N. Belov, S. A. Gavrilov, V. I. Shevyakov and E. N. Redichev, *Appl. Phys. A: Mater. Sci. Process.*, 2011, **102**, 219–223.

18 G. Sharma, M. V. Pishko and C. A. Grimes, *J. Mater. Sci.*, 2007, **42**, 4738–4744.

19 G. Riveros, S. Green, A. Cortes, H. Gomez, R. E. Marotti and E. A. Dalchiele, *Nanotechnology*, 2006, **17**, 561–570.

20 H. S. Shin, J. Yu and J. Y. Song, *Appl. Phys. Lett.*, 2007, **99**, 173106.

21 M. Michailov and D. Kashchiev, *J. Phys.: Conf. Ser.*, 2012, **398**, 012010.

22 H. S. Park, W. Cai, H. D. Espinosa and H. Huang, *MRS Bull.*, 2009, **34**, 178–183.

23 X. W. Wang, G. T. Fei, K. Zheng, Z. Jin and L. D. Zhang, *Appl. Phys. Lett.*, 2006, **88**, 173114.

24 Yu. I. Shilyaeva, V. V. Bardushkin, M. V. Silibin, S. A. Gavrilov, V. B. Yakovlev and O. V. Pyatilova, *Inorg. Mater.*, 2013, **49**, 676–680.

25 Yu. I. Shilyaeva, V. V. Bardushkin, M. V. Silibin, S. A. Gavrilov, V. B. Yakovlev and O. V. Pyatilova, *Russ. J. Phys. Chem. A*, 2013, **87**, 1870–1874.

26 H. Masuda and K. Fukuda, *Science*, 1995, **268**, 1466–1468.

27 Yu. D. Gamburg, *Galvanicheskie Pokrytiya. Spravochnik po Primeneniyu Galvanic coatings. Handbook of applications*, Tehnosfera, Moscow, 2006 [in Russian].

28 V. Bardushkin and V. Yakovlev, *Mechanics of Microstructures, Effective and Local Properties of Textured Polycrystals and Composites*, Lambert Academic, Saarbrüken, Germany, 2011 [in Russian].

29 A. P. Sychev and V. V. Bardushkin, *Mikromechanics of Tribocomposites*, Lambert Academic, Saarbrüken, Germany, 2013 [in Russian].

30 K. Lu and Y. Li, *Phys. Rev. Lett.*, 1998, **80**, 4474–4477.

31 G. Guisbiers and S. Pereira, *Nanotechnology*, 2007, **18**, 435710.

32 A. J. Kinloch, *Adhesion and Adhesives: Science and Technology*, Chapman and Hall, London, 1987.

33 *Fizicheskie Velichiny: Spravochnik, Physical Quantities: Handbook*, ed. I. S. Grigor'ev and E. Z. Meilikhov, Energoatomizdat, Moscow, 1991 [in Russian].

34 A. M. Korol'kov, *Litejnye Svojstva Metallov I Splavov, Casting Properties of Metals and Alloys*, Izd. Akad. Nauk USSR, Moscow, 1960 [in Russian].

35 Z. Xia, L. Riester, B. W. Sheldon, A. Curtin, J. Liang, A. Yin and J. M. Xu, *Rev. Adv. Mater. Sci.*, 2004, **34**, 131–139.

36 P. Gu, H. Miao, Z. T. Liu, X. P. Wu and J. H. Zhao, *J. Mater. Sci.*, 2004, **39**, 3369–3373.

37 L. Fernandez-Romero, J. M. Montero-Moreno, E. Pellicer, F. Peiro, A. Cornet, J. R. Morante, M. Sarret and C. Muller, *Mater. Chem. Phys.*, 2008, **111**, 542–547.

38 T. D. Shermergor, *Teoriya Uprugosti Mikroneodnorodnykh Sred, Theory of Elasticity of Microinhomogeneous Media*, Nauka, Moscow, 1977 [in Russian].

39 R. Hill, *J. Mech. Phys. Solids*, 1963, **11**, 357–372.

40 N. Laws, *J. Elasticity*, 1977, 7, 91–97.

41 H. J. Böhm, *A Short Introduction to Basic Aspects of Continuum Micromechanics*, Institute of Lightweight Design and Structural Biomechanics, Vienna University of Technology, Vienna, 2013.

42 L. P. Khoroshun, B. P. Maslov and P. V. Leshchenko, *Prognozirovanie effektivnykh svoistv p'ezoaktivnykh kompozitnykh materialov, Predicting Effective Properties of Piezoelectrically Active Composite Materials*, Naukova Dumka, Kiev, 1989 [in Russian].

43 Yu. I. Shilyaeva, V. V. Bardushkin and V. B. Yakovlev, *Jekologicheskij Vestnik Nauchnyh Centrov Chernomorskogo Jekonomicheskogo Sotrudnichestva*, 2013, **2**, 21–26 [in Russian].

44 V. V. Bardushkin, Yu. I. Shilyaeva and V. B. Yakovlev, *Deformacija I Razrushenie Materialov*, 2013, **10**, 24–29 [in Russian].

This journal is © the Owner Societies 2014

Phys. Chem. Chem. Phys., 2014, **16**, 19394–19401 | 19401